

LETTER TO THE EDITOR

The spatial distribution of an aromatic molecule, C_6H_5CN , in the cold dark cloud TMC-1[★]

J. Cernicharo¹, B. Tercero^{2,3}, N. Marcelino^{2,3}, M. Agúndez¹, and P. de Vicente²

¹ Dept. of Molecular Astrophysics, Instituto de Física Fundamental (IFF-CSIC), C/ Serrano 121, 28006 Madrid, Spain
e-mail: jose.cernicharo@csic.es

² Centro de Desarrollos Tecnológicos, Observatorio de Yebes (IGN), 19141 Yebes, Guadalajara, Spain

³ Observatorio Astronómico Nacional (OAN, IGN), Madrid, Spain

Received 21 April 2023; accepted 21 May 2023

ABSTRACT

We present a highly sensitive 2D line survey of TMC-1 obtained with the Yebes 40m radio telescope in the Q-band (31.13-49.53 GHz). These maps cover a region of $320'' \times 320''$ centred on the position of the QUIJOTE¹ line survey with a spatial sampling of $20''$. The region covering $240'' \times 240''$, where a longer integration time was used, shows a homogenous sensitivity of 2-4 mK across the band. We present in this work the first determination of the spatial extent of benzonitrile (C_6H_5CN), which follows that of cyanopolyynes rather well, but differs significantly from that of the radicals C_nH and C_nN . We definitively conclude that aromatic species in TMC-1 are formed from chemical reactions involving smaller species in the densest zones of the cloud.

Key words. molecular data – line: identification – ISM: molecules – ISM: individual (TMC-1) – astrochemistry

1. Introduction

In the last five years, two line surveys of the starless cold core TMC-1, QUIJOTE¹ (Cernicharo et al. 2020, 2021a, 2023) and GOTHAM² (McGuire et al. 2018, 2020), have been carried out and have provided the discovery of a panoply of new radicals, aromatic and polyaromatic compounds, cations, anions, and sulphur-bearing species. Roughly one-third of the molecules discovered in space have resulted from these two line surveys. The GOTHAM observations were taken with the Green Bank 100m radio telescope in the X-, K-, and Ka-bands. Most detections in this line survey were performed through a sophisticated statistical frequency stacking procedure. The QUIJOTE line survey is an ongoing line survey in the Q-band (31.1-50.3 GHz) obtained with the Yebes 40m radio telescope. The detection technique in QUIJOTE is the classical, and reliable, line-by-line detection without any spectral stacking. The present sensitivity of QUIJOTE is 0.12-0.25 mK (Cernicharo et al. 2023).

The modelling of this emission is often tackled with very limited information on the spatial extent of the observed emission. In GOTHAM and QUIJOTE the only available spatial information is provided by the variation of the telescope half power beam with the frequency across the line survey. While GOTHAM fits four velocity components with different spatial sizes, QUIJOTE assumes a source radius of $40''$ based on previous observations of TMC-1 in several molecular species. None of these methods is satisfactory to obtain the accurate column

densities needed to put constraints on the chemical models of the source. The spatial size of the observed molecules, together with the issues related to the line opacities and radiative transfer, can only be addressed through spatial mapping of the molecular emission.

To overcome these issues, the QUIJOTE line survey has been complemented with high-sensitivity maps obtained with the Yebes 40m radio telescope and covering a region of $320'' \times 320''$ centred on the QUIJOTE position (see Sect. 2). These maps are a faithful companion to the QUIJOTE line survey and we call these supplementary spatial data SANCHO.³ The goal of these maps is to permit the study of the spatial distribution of any QUIJOTE line with intensity ≥ 20 mK with a signal-to-noise ratio ≥ 10 , which means the low-energy transitions of most of the abundant species such as cyanopolyynes and radicals (C_nS , C_nH , and C_nN) among other molecules. Most of the isotopologues ^{13}C , ^{34}S , D , and ^{15}N of these species can be also spatially traced with SANCHO data.

In this letter we present the first determination of the spatial distribution of an aromatic molecule (benzonitrile, C_6H_5CN) in the starless cold dark cloud TMC-1, and compare it with that of other molecules.

2. Observations

New receivers, built within the Nanocosmos⁴ project and installed at the Yebes 40m radiotelescope, were used for the observations of TMC-1 ($\alpha_{J2000} = 4^h41^m41.9^s$ and $\delta_{J2000} = +25^\circ41'27.0''$). The present observations of TMC-1 complement

[★] Based on observations carried out with the Yebes 40m telescope (projects 22A007 and 22B029). The 40m radio telescope at Yebes Observatory is operated by the Spanish Geographic Institute (IGN, Ministerio de Fomento).

¹ Q-band Ultrasensitive Inspection Journey to the Obscure TMC-1 Environment

² GBT Observations of TMC-1: Hunting for Aromatic Molecules

³ Surveying the Area of the Neighbour TMC-1 Cloud through Heterodyne Observations

⁴ ERC grant ERC-2013-Syg-610256-NANOCOSMOS.
<https://nanocosmos.iff.csic.es/>

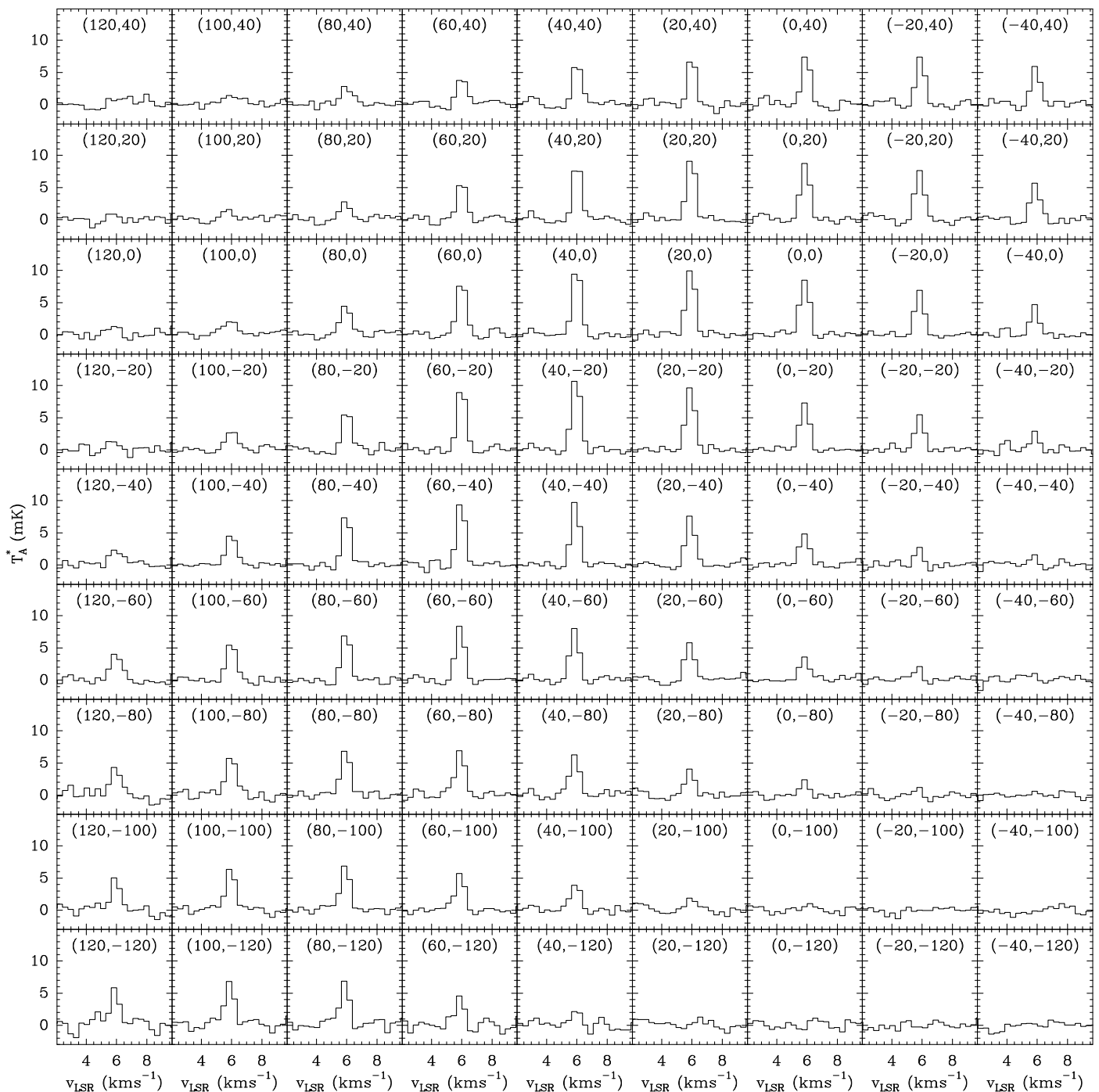


Fig. 1. Stacked line of C_6H_5CN obtained from the average in each position of 52 individual lines (see Appendix B). Only the spectra around the region of maximum emission (see Fig. 2) are shown. The offset positions in arcseconds are indicated in each panel. The abscissa in each panel corresponds to the local standard of rest velocity of the stacked data (in km s^{-1}). The intensity scale corresponds to the antenna temperature corrected for atmospheric transmission and antenna losses.

the QUIJOTE line survey (Cernicharo et al. 2021a). A detailed description of the telescope, receivers, and backends is given in Tercero et al. (2021). Briefly, the receiver consists of two cold high electron mobility transistor amplifiers covering the 31.1–50.3 GHz band with horizontal and vertical polarisations. Receiver temperatures in the first QUIJOTE observations achieved during 2020 vary from 22 K at 32 GHz to 42 K at 50 GHz. However, some power adaptation in the down-conversion chains in 2021 reduced the receiver temperatures to 16 K at 32 GHz and 25 K at 50 GHz. The backends are $2 \times 8 \times 2.5$ GHz fast

Fourier transform spectrometers (FFTs) with a spectral resolution of 38.15 kHz providing the whole coverage of the Q-band in both polarisations. The final Doppler correction was made during the pipeline processing of the raw data and the final spectra have the correct frequency scale in every part of the 31.1–50.3 GHz band.

The telescope beam size varies from $56.7''$ at 31 GHz to $35.6''$ at 49.5 GHz. The intensity scale used in this work, antenna temperature (T_A^*), was calibrated using two absorbers at different temperatures and the atmospheric transmission model

(ATM) (Cernicharo 1985; Pardo et al. 2001). Calibration uncertainties of 10 % were adopted. The beam efficiency of the Yebes 40m telescope in the Q-band is given as a function of frequency by $B_{\text{eff}}=0.797 \exp[-(\nu(\text{GHz})/71.1)^2]$. The forward telescope efficiency is 0.95.

The SANCHO maps were performed in the on-the-fly mode using frequency switching with a throw of 10 MHz. We prefer this observing mode as many molecular species have extended emission (Cernicharo & Guélin 1987). The speed of the telescope was 5"/sec and the data of the whole Q-band in the two polarisations were recorded every two seconds (16 individual spectra per position). The maps were done moving the telescope in right ascension from $-130''$ to $+130''$ with a declination step of $10''$. Once such a map was achieved, then the telescope was moved in declination from $-130''$ to $130''$ with a right ascension step of $10''$. This procedure was repeated until we reached 100 hours of observing time on the source. Some additional maps with a total observing time on source of 15 hours were added, covering offsets up to $\pm 160''$ in right ascension and declination. A total of 3468624 spectra, corresponding to 216789 different positions, two polarisations, and eight FFTs, were recorded in February and December 2022, and January 2023. The raw data file size is near 1 TByte. All data were analysed using the GILDAS package.⁵

3. Results

For the final SANCHO data, we produced six different types of maps that were obtained by resampling the raw data within a square grid with a point separation of $10''$ and $20''$ (S_{grid}), and with three different spatial tolerances around each position for adding raw data. These tolerance zones correspond to circles of $10''$, $15''$, and $20''$ in radius (T_{rad}). Each position in the maps contains the whole Q-band spectrum, with both polarisations averaged. The highest sensitivity is achieved for the maps with $S_{\text{grid}}=20''$ and $T_{\text{rad}}=20''$, which are those that we discuss in this work (see Appendix A). In this process no baseline is applied as the whole Q-band spectrum is treated simultaneously (31.13-49.53 GHz with 483928 channels at each position of the map). These maps are fully sampled spatially. However, due to the spatial tolerance used in creating the maps we expect to have produced some spatial smoothing (i.e. the emission in adjacent positions has some degree of correlation; see Appendix A).

Maps for each individual transition of a given molecule were obtained from the selected final map (with a given S_{grid} and T_{rad}) by extracting the spectral data over $\pm 14 \text{ km s}^{-1}$ around the frequency of the line. Transition frequencies were obtained from the spectral information of the MADEX code (Cernicharo 2012), the JPL catalogue (Pickett et al. 1998), or the CDMS database (Müller et al. 2005). A baseline is removed from each extracted spectrum after defining the windows for all lines potentially present in the selected velocity range using the QUIJOTE line survey as a reference for detected lines (only features above 5 mK were blanked in this process). Appendix A provides examples of several molecular lines at the central position of the map without and with baseline removal. The sensitivity over the Q-band as a function of frequency, T_{rad} , and position in the map is provided in Appendix A (see Table A.1).

It is worth noting that all maps produced in this way were observed simultaneously, and hence they have the same pointing and the same calibration uncertainties. Moreover, the relative calibration between different lines of a given molecule is much

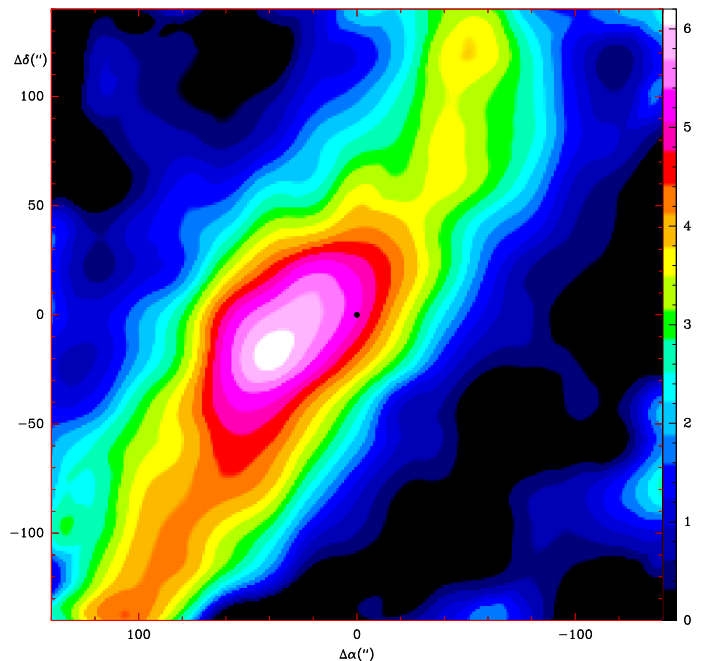


Fig. 2. Colour plot of spatial distribution of the integrated intensity between 5.3 and 6.5 km s^{-1} of the stacked lines of C₆H₅CN. The colour scale is in mK km s^{-1} . The sampling of the data is $20''$ and the integrating area in each position corresponds to a circle of $20''$ of radius. The black dot indicates the centre of the map, which corresponds to the position observed with the QUIJOTE line survey.

better than the global calibration uncertainty of 10 % (see e.g. Appendix A and Fig. A.1). The achieved sensitivity in each position depends on the adopted T_{rad} in adding data. In Appendix A we show the effect of adopting different gridding steps and tolerance circles. For $S_{\text{grid}}=20''$ and $T_{\text{rad}}=20''$, the sensitivity is 1.4-4 mK across the Q-band (the sensitivity is the same for $S_{\text{grid}}=10''$). This sensitivity is degraded by a factor of ~ 2 outside the square defined by $\Delta\alpha=\pm 120''$ and $\Delta\delta=\pm 120''$. Hence, SANCHO provides a whole spectrum of the Q-band over a map of 169 positions gridded every $20''$ ($240''\times 240''$) with a sensitivity that is similar to that achieved by GOTHAM in a single position. However, the sensitivity towards the centre of the map is worse by a factor of 10 compared to that of the QUIJOTE line survey.

The sensitivity reached by SANCHO allows the detection of all lines with intensities greater than 10 mK in the central position of the maps. This is enough to detect many of the lines of C₆H₅CN observed with the QUIJOTE line survey presented in Fig. B.1 of Cernicharo et al. (2021b). However, the spatial distribution of the integrated intensity of each individual line appears noisy, which prevents us from reaching a conclusion on the spatial extent of this aromatic species. We therefore used the maps generated for each individual line to produce a spectrally stacked map. We added 49 lines of benzonitrile which are free of resolved hyperfine structure and of blending with lines from other species (see Table B.1). Each line was multiplied by a factor to take into account the observed intensity with respect to a reference line, the strongest one of benzonitrile in the QUIJOTE line survey (the $13_{0,13}-12_{0,12}$ transition at 32833.827 MHz). The procedure is described in detail in Appendix B. The stacking scheme allows one to use the parameters of the reference line to estimate the column density and increases the S/N of the stacked spectral map with respect the observed individual line maps of benzonitrile.

⁵ <http://www.iram.fr/IRAMFR/GILDAS>

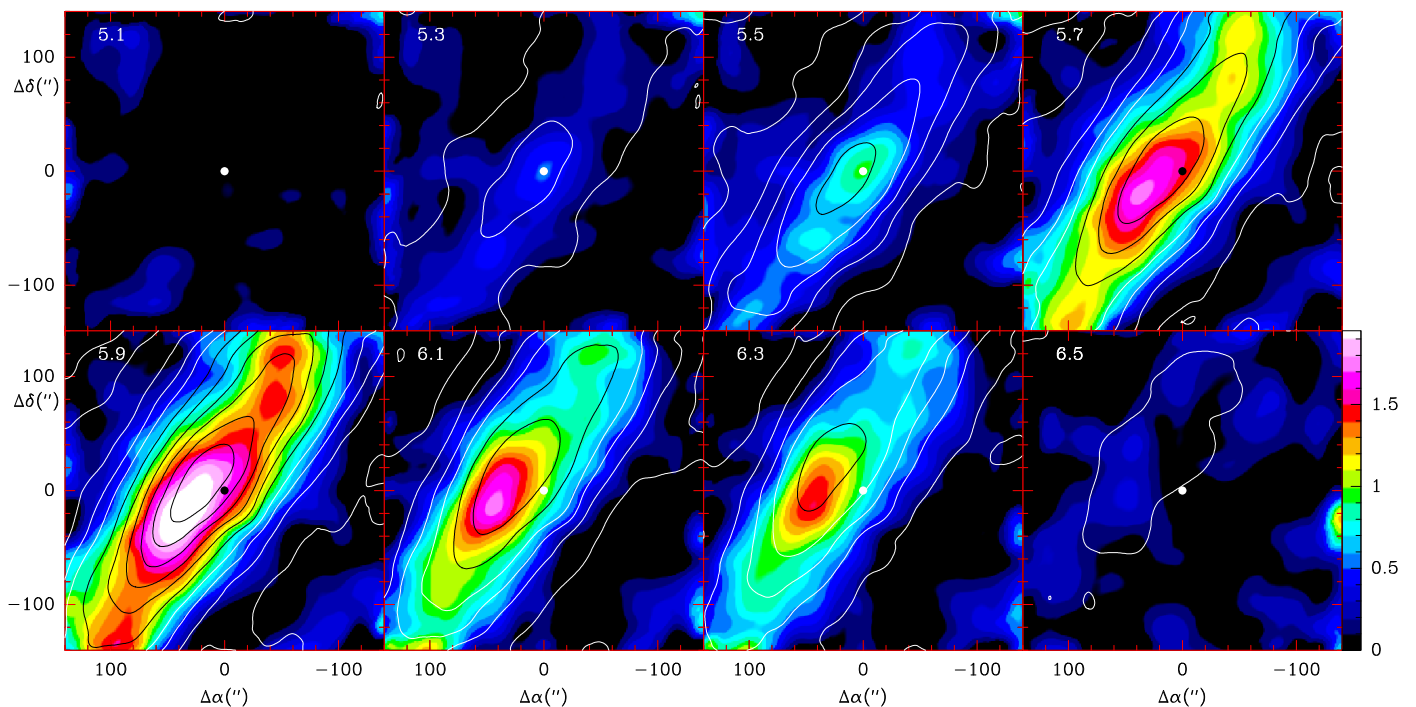


Fig. 3. Spatial distribution of the integrated intensity of the stacked lines of C_6H_5CN at different velocities. The selected velocity range is ± 0.1 $km\ s^{-1}$ around the velocity indicated in the upper right corner of each panel (in $km\ s^{-1}$). The sampling of the data is $20''$ and the integrating area in each position corresponds to a circle of $20''$ radius. The white and black contours represent the integrated intensity of the $J=28-27$ transition of HC_7N at the same velocity (± 0.1 $km\ s^{-1}$). The first white contour corresponds to 2 $mK\ km\ s^{-1}$ and the step is 4 $mK\ km\ s^{-1}$. The first black contour corresponds to 20 $mK\ km\ s^{-1}$ and the step is 6 $mK\ km\ s^{-1}$. The white or black dot indicates the centre of the map.

The resulting spectra at different positions in the map are shown in Fig. 1. The sensitivity of the map of the stacked lines at the $(\Delta\alpha, \Delta\delta)$ positions $(0'', 0'')$, $(120'', 0'')$, and $(120'', -120'')$ is 0.4 mK , 0.6 mK , and 0.9 mK , respectively (see Fig. 1). The spatial distribution of the integrated intensity of this aromatic species is shown in Fig. 2. Finally, the spatial distribution of the emission at different velocities is shown in Fig. 3.

4. Discussion

The comparison of the velocity maps of C_6H_5CN and HC_7N shown in Fig. 3 clearly indicates that the two species coexist spatially. The emission of the two species covers the velocity range $5.3-6.3$ $km\ s^{-1}$, with some weak emission still at 6.5 $km\ s^{-1}$. The observed emission follows the well-known filamentary structure of TMC-1 with a dense condensation around the central position. Two different velocities seem to be traced spatially by our data, both with a filamentary aspect: one at 5.5 $km\ s^{-1}$ with its maximum over the QUIJOTE position (known as the cyanopolyynes source) and the other at 5.9 $km\ s^{-1}$ that peaks at $\Delta\alpha=40''$ and $\Delta\delta=-20''$, which dominates the line profile. Given our velocity resolution of ~ 0.25 $km\ s^{-1}$, the observed velocity structure could also be interpreted as resulting from a velocity gradient perpendicular to the TMC-1 filament, or as a twisting motion of filaments, or fibres, similar to those found in other molecular clouds (Kirk et al. 2013; Hacar et al. 2013, 2017). This behaviour is similar for all the species we study in this work. The TMC-1 filament was observed in the emission of molecules such as SO , NH_3 , and CCS , with higher spatial resolution than we used (see e.g. Lique et al. 2006; Fehér et al. 2016; Dobashi et al. 2019, and references therein). These authors found a complex spatial velocity structure dominated by clumpy filaments at velocities between 5.3 and 6.3 $km\ s^{-1}$.

The spatial coexistence of benzonitrile and other molecules is fully confirmed in Fig. 4, where we compare the spatial distribution of the integrated intensity of several species, including radicals, cyanopolyynes, methyl-bearing species, and isomers of HC_3N . This is the first time that many of the selected molecules have been mapped in TMC-1. Moreover, the signal-to-noise ratio of all these maps is extremely high as the selected lines have intensities ≥ 100 mK , even for the HC_7N $J=38-37$ for which the upper level energy is 40.1 K . The integrated intensities are proportional to the column densities because the lines are mostly optically thin. The map of HC_3N was obtained using the integrated intensity of the weak satellite hyperfine lines, which also guarantees low line opacities.

Opacity effects, the beam size of the telescope, different excitation conditions, and the spatial smearing produced by the co-addition of the on-the-fly data could produce some small differences between the maps. However, some of these differences are real and are related to the global aspect of the spatial distribution. For example, cyanopolyynes and benzonitrile are significantly shifted towards the north-east by more than a beam with respect to the radicals C_nH and C_nN . The spatial shift of the radicals C_4H , C_6H , and C_3N with respect to the cyanopolyynes HC_3N and HC_5N may be caused by the structure of the H_2 density. The HC_3N peak is also a local maximum in H_2 density (see Pratap et al. 1997), and radicals are probably more efficiently destroyed at high densities than closed-shell molecules. A different spatial distribution was also found in TMC-1 by Fossé et al. (2001) for C_6H , $c-C_3H_2$, and H_2C_3 . Significant differences are also found for the two transitions of HC_7N shown in Fig. 4. This is probably due to the high energy of the $J=38$ level, which renders this transition very sensitive to the density or to small changes in the kinetic temperature. The analysis of the spatial distribution

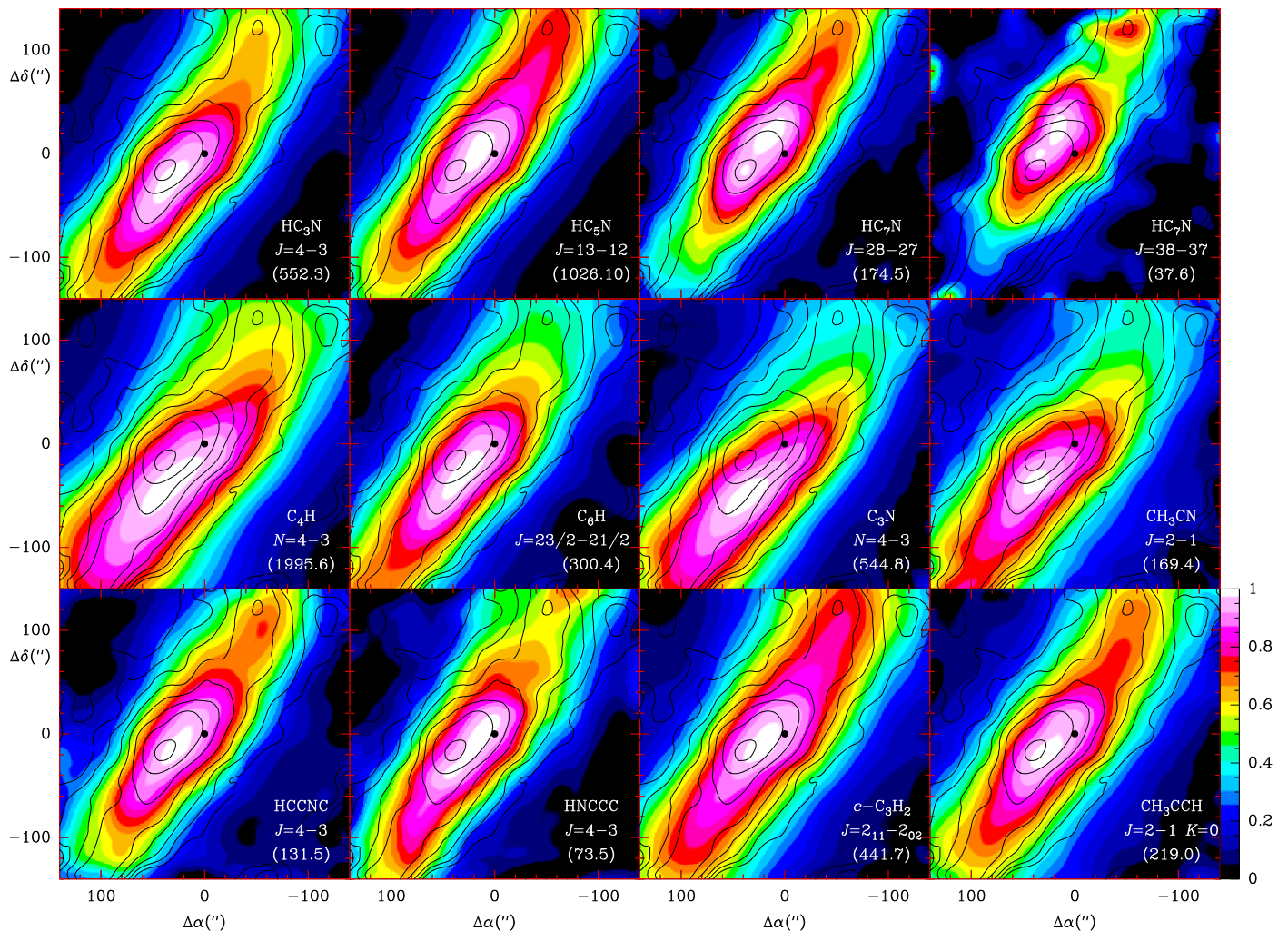


Fig. 4. Integrated intensity between 5.3 and 6.5 km s⁻¹ of different molecular transitions (colours) compared with that of C₆H₅CN (black contours; first contour and step are 0.75 mK km s⁻¹). For each molecular transition the integrated intensity has been normalised to the maximum value within the area covered by the map. The colour scale (bottom right) is the same for all molecular transitions. The molecule, transition, and maximum intensity (shown in brackets) are indicated in the bottom right corner of each panel. The black dot corresponds to the centre of the map.

of several transitions of radicals, cyanopolyynes, hydrocarbons, and their isotopologues will be published in forthcoming papers.

The formation of aromatic cycles in TMC-1 has been a matter of debate in recent years (McGuire et al. 2018, 2021; Cernicharo et al. 2021b, 2022). It is not yet clear whether these aromatic rings are formed through a bottom-up mechanism or a top-down process. The presence of large polycyclic aromatic hydrocarbons (PAHs) in diffuse interstellar clouds is inferred from the observation of intense unidentified infrared bands, and the aromatic cycles observed in TMC-1 could result from the destruction of this reservoir of PAHs inherited from a previous diffuse stage. A similar process has been invoked to account for the formation of small hydrocarbons in photodissociation regions (Pety et al. 2005). Alternatively, aromatic rings could be formed from small hydrocarbons in a bottom-up process. For example, the reaction of propene, an abundant hydrocarbon in TMC-1 (Marcelino et al. 2007), with CH can produce 1,3-butadiene (Loison & Bergeat 2009), which can lead to *c*-C₅H₇ upon reaction with CH (Cernicharo et al. 2021b) and to benzene by reacting with C₂H (Jones et al. 2011). Even so, chemical models based on these neutral-neutral routes are not able to account for the observed abundances of cycles such as *c*-C₅H₇ (Cernicharo et al. 2022), which indicates that ion-neutral reac-

tions may also play a role in the synthesis of aromatic cycles. Whatever the true mechanism of formation of aromatic rings, the fact that benzonitrile has a spatial distribution very similar to that of cyanopolyynes supports the argument that aromatic molecules are formed through a bottom-up chemical process, as is thought to occur for long carbon chains in TMC-1.

5. Conclusions

We have presented the SANCHO maps of TMC-1 in the frequency range 31.13–49.53 GHz. The sensitivity of the spectra over an area of 240''×240'', for a gridding step of 20'' and $T_{rad}=20''$, is 2–4 mK across the band. We have determined, for the first time, the spatial distribution of C₆H₅CN (benzonitrile). We find that it correlates very well with that of cyanopolyynes, and that it extends over the TMC-1 filament. Hence, we conclude that this species is formed through bottom-up chemical processes involving the same type of reactions as those forming the other species found in the cloud.

Acknowledgements. We thank ERC for funding through grant ERC-2013-SyG-610256-NANOCOSMOS. We also thank Ministerio de Ciencia e Innovación of Spain (MICIU) for funding support through projects PID2019-106110GB-

I00, PID2019-107115GB-C21 / AEI / 10.13039/501100011033, and PID2019-106235GB-I00.

References

- Agúndez, M., Cabezas, C., Tercero, B., et al. 2021, A&A, 647, L10
- Cernicharo, J. 1985, Internal IRAM report (Granada: IRAM)
- Cernicharo, J., Guélin, M., 1987, A&A, 183, L10
- Cernicharo, J., 2012, in ECLA 2011: Proc. of the European Conference on Laboratory Astrophysics, EAS Publications Series, 2012, Ed.: C. Stehl, C. Joblin, & L. d'Hendecourt (Cambridge: Cambridge Univ. Press), 251; https://nanocosmos.iff.csic.es/?page_id=1619
- Cernicharo, J., Marcelino, N., Agúndez, M. et al. 2020, A&A, 642, L8
- Cernicharo, J., Agúndez, M., Kaiser, R., et al. 2021a, A&A, 652, L9
- Cernicharo, J., Agúndez, M., Kaiser, R.I. et al. 2021b, A&A, 655, L1
- Cernicharo, J., Fuentetaja, R., Agúndez, M., et al. 2022, A&A, 663, L9
- Cernicharo, J., Pardo, J.R., Cabezas, C. et al. 2023, A&A, 670, L19
- Dobashi, K., Shimoikura, T., Ochiai, T. et al. 2019, ApJ, 879:88
- Fehér, O., Tóth, L.V., Ward-Thompson, D. et al. 2016, A&A, 590, A75
- Fossé, D., Cernicharo, J., Gerin, M., Cox, P. 2001, ApJ, 552, 168
- Hacar, A., Tafalla, M., Kauffmann, J. & Kovács, A. 2013, A&A, 554, A55
- Hacar, A., Tafalla, M. & Alves, J. 2017, A&A, 606, A123
- Jones, B. M., Zhang, F., & Kaiser, R. I. 2011, PNAS, 108, 452
- Kirk, H., Myers, P.C., Bourke, T.L. et al. 2012, ApJ, 766, 115
- Lique, F., Cernicharo, J. & Cox, P. 2006, ApJ, 653, 1342
- Loison, J.-C. & Bergeat, A. 2009, PCCP, 11, 655
- Marcelino, N., Cernicharo, J., Agúndez, M. et al. 2007, ApJ, 665, L127
- McGuire, B. A., Burkhardt, A. M., Kalenskii, S., et al. 2018, Science, 359, 202
- McGuire, B. A., Burkhardt, A. M., Loomis, R. A., et al. 2020, ApJ, 900, L10
- McGuire, B. A., Loomis, R. A., Burkhardt, A. M., et al. 2021, Science, 371, 1265
- Müller, H.S.P., Schlöder, F., Stutzki, J., Winnewisser, G. 2005, J. Mol. Struct., 742, 215
- Pardo, J. R., Cernicharo, J., Serabyn, E. 2001, IEEE Trans. Antennas and Propagation, 49, 12
- Pety, J., Teyssier, D., Fossé, D., et al. 2005, A&A, 435, 885
- Pickett, H.M., Poynter, R. L., Cohen, E. A., et al. 1998, J. Quant. Spectrosc. Radiat. Transfer, 60, 883
- Pratap, P., Dickens, J.E., Snell, R.L. et al. 1997, ApJ, 486, 862
- Tercero, F., López-Pérez, J. A., Gallego, et al. 2021, A&A, 645, A37

Table A.1. Sensitivity of the maps as a function of the frequency and of the distance to the central position.

| Frequency (MHz) | $\sigma(10'')$ ^a (mK) | | | $\sigma(15'')$ ^a (mK) | | | $\sigma(20'')$ ^a (mK) | | |
|--------------------|-------------------------------------|-----|------|-------------------------------------|-----|------|-------------------------------------|-----|-----|
| | P1 | P2 | P3 | P1 | P2 | P3 | P1 | P2 | P3 |
| 31120 | 3.6 | 4.7 | 7.4 | 3.2 | 3.4 | 6.0 | 2.3 | 2.6 | 4.5 |
| 31500 | 2.6 | 3.8 | 6.1 | 2.3 | 2.8 | 4.9 | 1.9 | 2.0 | 3.6 |
| 32500 | 2.2 | 3.2 | 6.2 | 2.0 | 2.9 | 4.8 | 1.4 | 1.6 | 3.2 |
| 33500 | 2.2 | 2.8 | 3.9 | 1.9 | 2.1 | 3.7 | 1.3 | 1.6 | 2.7 |
| 34500 | 2.5 | 3.0 | 5.0 | 2.2 | 2.8 | 4.1 | 1.6 | 1.9 | 3.2 |
| 35500 | 2.5 | 2.6 | 4.8 | 2.3 | 2.2 | 4.2 | 1.7 | 1.8 | 2.9 |
| 36500 | 2.2 | 3.2 | 5.9 | 2.2 | 2.7 | 5.0 | 1.5 | 2.0 | 3.2 |
| 37500 | 2.6 | 3.3 | 5.8 | 2.4 | 2.9 | 4.9 | 1.7 | 1.9 | 3.2 |
| 38500 | 2.7 | 3.5 | 6.0 | 2.3 | 3.3 | 5.3 | 1.6 | 2.2 | 3.9 |
| 39500 | 2.9 | 3.5 | 6.1 | 2.5 | 3.1 | 5.2 | 2.0 | 1.9 | 4.2 |
| 40500 | 2.9 | 4.0 | 6.3 | 2.6 | 3.3 | 4.7 | 1.9 | 2.1 | 3.9 |
| 41500 | 3.4 | 4.1 | 7.3 | 3.1 | 3.6 | 5.6 | 2.1 | 2.5 | 4.2 |
| 42500 | 3.3 | 3.8 | 6.8 | 2.9 | 3.6 | 5.6 | 2.2 | 2.5 | 4.3 |
| 43500 | 3.7 | 5.2 | 6.1 | 3.2 | 3.9 | 5.5 | 2.1 | 2.8 | 4.5 |
| 44500 | 3.2 | 5.1 | 6.9 | 2.9 | 4.3 | 6.4 | 2.2 | 3.2 | 4.7 |
| 45500 | 3.8 | 5.6 | 8.4 | 3.5 | 4.7 | 7.4 | 2.9 | 3.4 | 6.0 |
| 46500 | 4.1 | 6.4 | 9.1 | 3.9 | 5.4 | 7.4 | 2.9 | 3.9 | 6.3 |
| 47500 | 5.5 | 7.6 | 10.0 | 4.9 | 6.8 | 9.0 | 3.5 | 4.8 | 7.8 |
| 48500 | 6.3 | 7.8 | 11.6 | 5.8 | 6.9 | 9.4 | 3.7 | 4.7 | 7.7 |
| 49000 | 6.2 | 7.1 | 12.2 | 5.5 | 6.2 | 10.8 | 3.9 | 4.6 | 8.3 |
| 49500 | 6.3 | 7.1 | 12.1 | 5.7 | 6.5 | 10.5 | 4.0 | 4.7 | 7.8 |

Notes.

The three selected positions in the map, P1, P2, and P3, correspond to the central position $\Delta\alpha=0''$, $\Delta\delta=0''$, to offset $\Delta\alpha=100''$, $\Delta\delta=0''$, and to offset $\Delta\alpha=120''$, $\Delta\delta=-120''$, respectively.

^(a) Root mean square noise derived from a polynomial baseline removal to a frequency range of ± 3 MHz (157 channels) around each selected frequency. The value adopted for T_{rad} is indicated in brackets.

Appendix A: Baselines, gridding step, tolerance circle, and sensitivity

Our on-the-fly frequency switching observations suffer from frequency ripples. However, the period of these ripples is always larger than 10 MHz, while the lines in the Q-band are typically 0.10-0.18 MHz wide. Hence, it is possible to remove a polynomial baseline to each line of the survey at each position of the map with total confidence that neither the line intensity nor the line profile are perturbed by the baseline removal step. These effects are also present in the QUIJOTE line survey, and we follow a procedure similar to that previously described for these frequency switching observations (Cernicharo et al. 2022).

An example of the baseline removal procedure in the SANCHO maps is shown in Fig. A.1 where we consider the $N=4-3$ and $N=5-4$ transitions of CCCN. These lines exhibit two line components separated by ~ 19 MHz due to the fine structure of the rotational transitions. The lines are shown in Fig. A.1 before and after baseline subtraction. For the $N=4-3$ transition the derived sensitivity is 2 mK. The observed intensity ratio of the two fine components is 1.35, while the theoretical value is 1.33 (for optically thin emission). For the two components of the $N=5-4$ transition the derived sensitivity is 4.2 mK and the line strength ratio is 1.21, which is very close to the theoretical value of 1.24. The number of channels in Fig. A.1 is 630.

The folding of the frequency switching data can produce negative features that could affect the intensity and line profile of some of the observed lines. However, at the level of sensi-

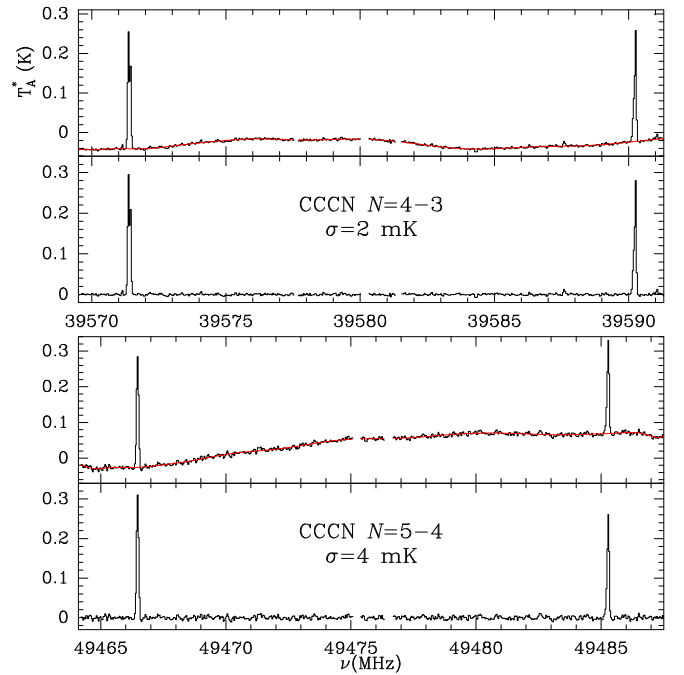


Fig. A.1. Observed lines of CCCN before and after baseline subtraction. For each transition of CCCN the upper panel shows the raw data and the fitted baseline (red line) at the centre position of the map with $S_{grid}=20''$ and $T_{rad}=20''$. The panel below each transition shows the data after a polynomial baseline removal.

tivity of SANCHO (2-4 mK) only a few lines with intensities greater than 10 mK could be affected by this issue. However, at better sensitivities, such as those of the QUIJOTE line survey (Cernicharo et al. 2020, 2021a, 2023), this effect could be a concern and is mitigated by the use of two sets of data with different frequency switching throws and similar sensitivity.

The effect of the gridding step and tolerance circle on the final aspect of the maps was analysed with the $J=28-27$ transition of HC₇N at 31583.709 MHz (beam size 56''), and the $J=1-0$ line of C³⁴S at 48206.942 MHz (beam size 39''). Values of $S_{grid}=10''$ and $20''$, and $T_{rad}=10''$, $15''$, and $20''$ were used. These maps are shown in Fig. A.2.

For HC₇N both values of S_{grid} produce oversampled maps. When T_{rad} is changed from $10''$ to $20''$ the maps show a better aspect, but as a counterpart a considerable spatial smoothing (smearing) is introduced, together with a small dilution of the maximum intensity. The same applies to the maps of C³⁴S, which are fully sampled in this case. Depending on the physical parameters we want to study, different values of S_{grid} and T_{rad} can be used depending on the intensity of the mapped lines and on the desired signal-to-noise ratio in each position on the maps. For weak lines the spatial shape of the emission could be analysed with $T_{rad}=20''$, while the maps for lines with intensity greater than 100 mK, $T_{rad}=10''$ or $15''$ could be better adapted. In this work we focus on the study of the extended emission of the weak lines of benzonitrile, and hence we adopt $T_{rad}=20''$ and $S_{grid}=20''$.

We estimated the sensitivity of the adopted values of S_{grid} and T_{rad} by selecting 21 frequencies across the Q-band. A range of ± 3 MHz (157 channels) was selected. Three different positions are considered at distances from the centre of the map of $0''$, $100''$, and $170''$. The results are given in Table A.1.

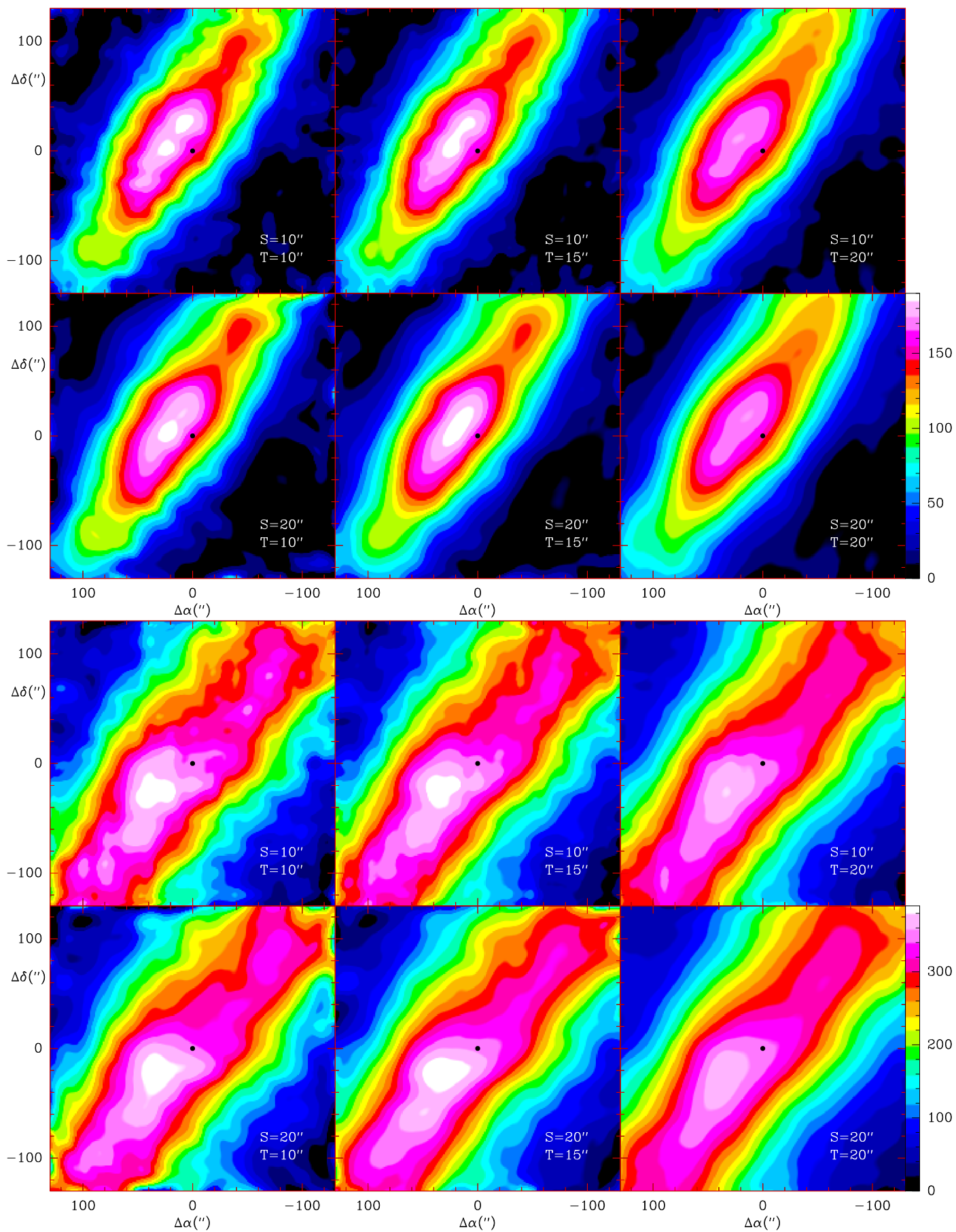


Fig. A.2. Integrated intensity of the $J=28-27$ transition of HC_7N (upper panels) and $\text{C}^{34}\text{S } J=1-0$ (lower panels) for different values of S_{grid} and T_{rad} . The telescope beam size for the two transitions is $56''$ and $39''$, respectively. The black dot indicates the centre of the maps. The maximum value of the integrated intensity changes by less than 10% from $T_{\text{rad}}=10''$ to $20''$.

Appendix B: Maps of C₆H₅CN

In order to spectrally stack the lines of C₆H₅CN and to produce a high signal-to-noise ratio map of its spatial distribution, we defined a selection criterion of the lines to be stacked at each position of the maps. The intensity of all lines of benzonitrile in TMC-1 in the Q-band are below 10 mK (Cernicharo et al. 2021b). Some of these lines have an intensity of 1-2 mK which is well below the detection sensitivity of the maps with $T_{rad}=20''$ (see Table A.1). In addition, several of these lines show hyperfine structure (see Fig. B.1 of Cernicharo et al. 2021b). We used the last product of the QUIJOTE line survey (Cernicharo et al. 2023) to select all lines of benzonitrile that appear as a single feature and are free of blending from other lines. The QUIJOTE data were also used to define the windows for baseline removal for each of the selected lines.

A second selection criterion was the intensity of the lines relative to the strongest one that was taken as reference (the 13_{0,13}-12_{0,12} transition). Only lines with one-third of the intensity of the reference line in the QUIJOTE data were selected. The final list of lines used for stacking corresponds to the 49 transitions given in Table B.1. This table also provides the measured intensity of the lines with QUIJOTE (Cernicharo et al. 2023) and the applied multiplicative factor for stacking. This multiplicative factor scales all lines to the intensity of the reference line. The data were weighted by $1/\sigma^2$, where σ is the measured sensitivity of each line after multiplication by the intensity scale factor. Hence, we can add lines scaled to the same intensity to produce a stacked spectrum at each position of the map. Most of the selected lines are seen in the central position of the map without stacking, but with a limited signal-to-noise ratio. Figure B.1 shows a sub-sample of the selected transitions at the centre position. The multiplicative factor and the measured sensitivity (after multiplication to scale the signal to that of the reference line), are indicated in each panel (see also Table B.1).

The final stacked spectra are shown in Fig. 1. The improvement of sensitivity after stacking is a factor of 3.5 with respect to that of the unstacked strongest lines.

Table B.1. Lines of C₆H₅CN used for spectral stacking at each position.

| Transition | Frequency (MHz) | T _A [*] (mK) | f _{mul} ^b |
|--|-----------------|----------------------------------|-------------------------------|
| 11 _{2,9} -10 _{2,8} | 32023.223 | 9.7 | 1.05 |
| 12 _{2,11} -11 _{2,10} | 32314.461 | 8.8 | 1.16 |
| 13 _{1,13} -12 _{1,12} | 32763.506 | 8.4 | 1.21 |
| 13 _{0,13} -12 _{0,12} | 32833.827 | 10.2 | 1.00 |
| 12 _{1,11} -11 _{1,10} | 33249.003 | 6.2 | 1.65 |
| 12 _{3,10} -11 _{3,9} | 33336.175 | 4.6 | 2.43 |
| 12 _{3,9} -11 _{3,8} | 34389.613 | 4.3 | 2.37 |
| 13 _{2,12} -12 _{2,11} | 34864.915 | 8.9 | 1.15 |
| 12 _{2,10} -11 _{2,9} | 34898.780 | 10.1 | 1.01 |
| 14 _{1,14} -13 _{1,13} | 35202.608 | 5.9 | 1.73 |
| 14 _{0,14} -13 _{0,13} | 35249.171 | 10.1 | 1.01 |
| 13 _{1,12} -12 _{1,11} | 35661.310 | 6.1 | 1.67 |
| 13 _{3,11} -12 _{3,10} | 36066.955 | 4.3 | 2.37 |
| 13 _{4,10} -12 _{4,9} | 36321.233 | 5.1 | 2.00 |
| 13 _{4,9} -12 _{4,8} | 36539.047 | 5.0 | 2.04 |
| 14 _{2,13} -13 _{2,12} | 37391.925 | 8.3 | 1.23 |
| 13 _{3,10} -12 _{3,9} | 37477.470 | 4.4 | 2.32 |
| 15 _{1,15} -14 _{1,14} | 37638.179 | 6.0 | 1.70 |
| 15 _{0,15} -14 _{0,14} | 37668.578 | 9.3 | 1.10 |
| 13 _{2,11} -12 _{2,10} | 37709.061 | 9.8 | 1.04 |
| 14 _{1,13} -13 _{1,12} | 38038.711 | 5.7 | 1.79 |
| 14 _{3,12} -13 _{3,11} | 38772.958 | 4.4 | 2.32 |
| 14 _{4,11} -13 _{4,10} | 39147.318 | 5.5 | 1.85 |
| 14 _{4,10} -13 _{4,9} | 39501.269 | 4.6 | 2.22 |
| 15 _{2,14} -14 _{2,13} | 39897.901 | 8.9 | 1.15 |
| 16 _{1,16} -15 _{1,15} | 40071.306 | 5.2 | 1.96 |
| 16 _{0,16} -15 _{0,15} | 40090.922 | 8.3 | 1.23 |
| 15 _{1,14} -14 _{1,13} | 40401.006 | 4.7 | 2.17 |
| 14 _{2,12} -13 _{2,11} | 40445.137 | 9.9 | 1.03 |
| 14 _{3,11} -13 _{3,10} | 40564.446 | 4.5 | 2.27 |
| 15 _{4,12} -14 _{4,11} | 41967.092 | 5.0 | 2.04 |
| 16 _{2,15} -15 _{2,14} | 42385.689 | 7.8 | 1.31 |
| 17 _{1,17} -16 _{1,16} | 42502.779 | 4.3 | 2.37 |
| 15 _{4,11} -14 _{4,10} | 42513.064 | 5.9 | 1.73 |
| 17 _{0,17} -16 _{0,16} | 42515.315 | 7.1 | 1.44 |
| 16 _{1,15} -15 _{1,14} | 42762.895 | 4.1 | 2.49 |
| 15 _{2,13} -14 _{2,12} | 43099.531 | 7.8 | 1.31 |
| 15 _{3,12} -14 _{3,11} | 43625.762 | 4.4 | 2.32 |
| 16 _{4,13} -15 _{4,12} | 44775.824 | 4.7 | 2.17 |
| 18 _{0,18} -17 _{0,17} | 44941.103 | 6.9 | 1.48 |
| 17 _{1,16} -16 _{1,15} | 45132.664 | 4.7 | 2.17 |
| 16 _{4,12} -15 _{4,11} | 45576.805 | 4.8 | 2.13 |
| 16 _{2,14} -15 _{2,13} | 45668.515 | 6.9 | 1.48 |
| 17 _{3,15} -16 _{3,14} | 46721.270 | 3.5 | 2.91 |
| 18 _{2,17} -17 _{2,16} | 47318.725 | 4.5 | 2.27 |
| 19 _{0,19} -18 _{0,18} | 47367.825 | 5.6 | 1.82 |
| 18 _{1,17} -17 _{1,16} | 47513.403 | 3.5 | 2.91 |
| 17 _{4,14} -16 _{4,13} | 47568.715 | 3.5 | 2.91 |
| 17 _{2,15} -16 _{2,14} | 48155.082 | 5.3 | 1.92 |

Notes.

Selected transitions to generate the map of benzonitrile (C₆H₅CN).

^(a) Observed intensity in the QUIJOTE line survey in mK.

^(b) Applied multiplicative factor to the individual map of each selected transition.

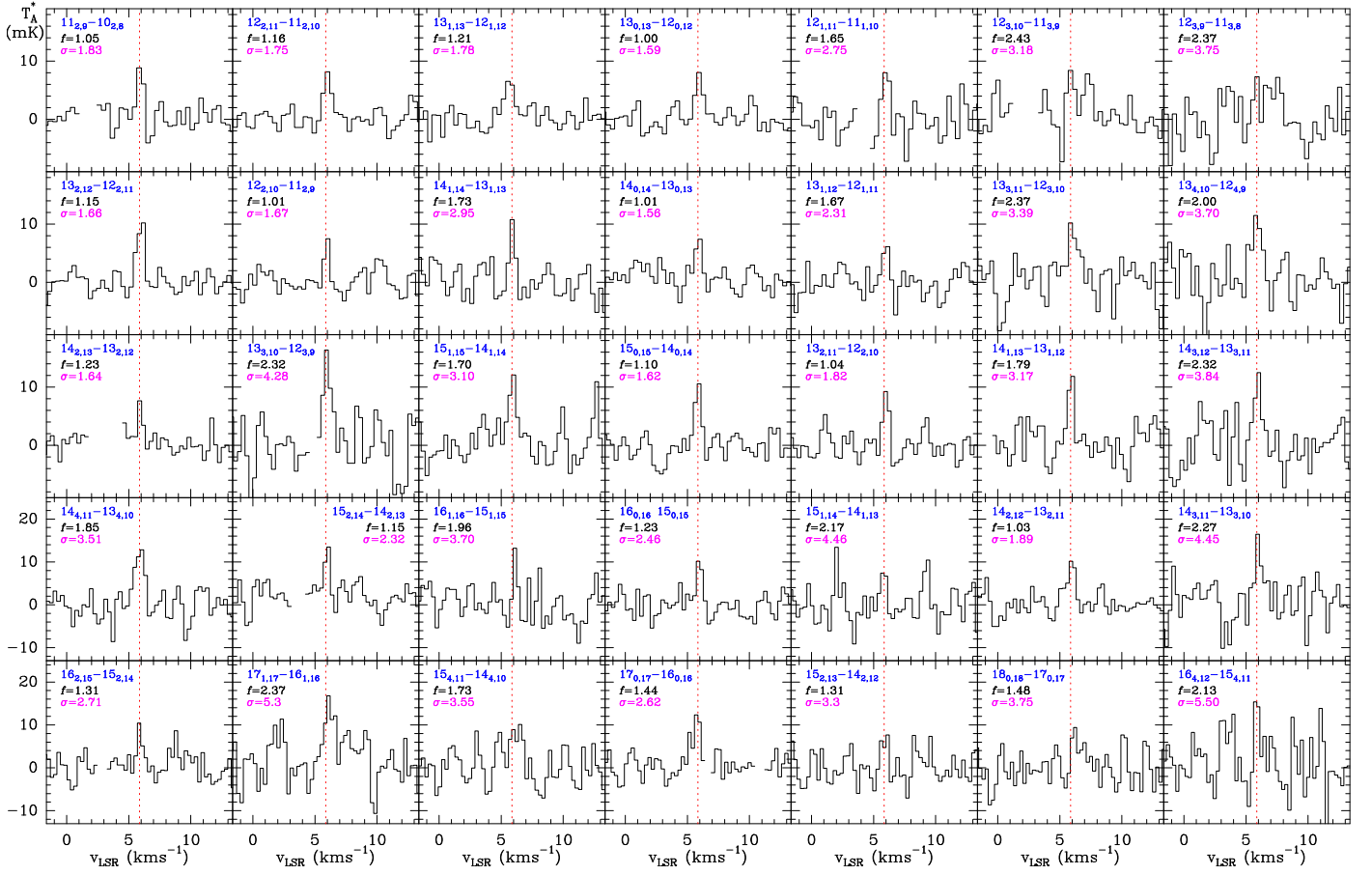


Fig. B.1. Selected transitions of C_6H_5CN among the 49 lines (see Table B.1) used to produce the spectrally stacked map of benzonitrile at each position of the map. The spectra shown here correspond to the central position. The transition quantum numbers are indicated in blue in the top left corner of each panel. Each line arises from the individual maps with $S_{grid}=20''$ and $T_{rad}=20''$. Each line spectrum was multiplied by the factor f (shown in black in each panel) to scale its intensity to that of the strongest one (the $13_{0,13}-12_{0,12}$ transition). The noise of each spectra, after multiplication by f , is shown in violet (σ ; in mK). It is used to weight the data during stacking of all the lines at each position of the map (see text). The vertical dashed red lines in each panel indicate the local standard of rest velocity of 5.86 km s^{-1} . The spectra of the resulting stacked data at different positions of the map are shown in Fig. 1.